PASJ: Publ. Astron. Soc. Japan **60**, 465–473, 2008 June 25

The 2006 Radio Outbursts of a Microquasar Cygnus X-3: Observations and Data

Masato TSUBOI, Tomoka TOSAKI, Nario KUNO, Kouichiro NAKANISHI, Tsuyoshi SAWADA, and Tomofumi UMEMOTO
Nobeyama Radio Observatory, 462-2 Nobeyama, Minamimaki, Minamisaku, Nagano 384-1305*
Sergei A. TRUSHKIN
Special Astrophysical Observatory RAS, Nizhnij Arkhyz, Karachaevo-Cherkassia 369167, Russia
Taro KOTANI and Nobuyuki KAWAI
Department of Physics, Tokyo Institute of Technology, 2-12-1 Ookayama, Meguro-ku, Tokyo 152-8551
Yasutaka KURONO, Toshihiro HANDA, and Kotaro KOHNO
Institute of Astronomy, School of Science, The University of Tokyo, 2-21-1 Osawa, Mitaka, Tokyo 181-8588
Takashi TSUKAGOSHI
The Graduate University for Advanced Studies (Sokendai), 2-21-1 Osawa, Mitaka, Tokyo 181-8588
Osamu KAMEYA and Hideyuki KOBAYASHI
Mizusawa VERA Observatory, 2-12 Hoshigaoka, Mizusawa, Oshu, Iwate 023-0861
Kenta FUJISAWA and Akihiro DOI
Faculty of Science, Yamaguchi University, 1677-1 Yoshida, Yamaguchi, Yamaguchi 753-8512
Toshihiro OMODAKA
Faculty of Science, Kagoshima University, 1-21-35 Kôrimoto, Kagoshima, Kagoshima 890-0065
Hiroshi TAKABA, Hiroshi SUDOU, and Ken-ichi WAKAMATSU
Faculty of Engineering, Gifu University, 1-1 Yanagido, Gifu 501-1193
Yasuhiro KOYAMA and Eiji KAWAI
Kashima Space Research Center, National Institute of Information and Communications Technology, 893-1 Hirai, Kashima, Ibaraki 314-8501
and
Nanako MOCHIZUKI and Yasuhiro MURATA
Institute of Space and Astronautical Science, JAXA, 3-1-1 Yoshinodai, Sagamihara, Kanagawa 229-8510

(Received 2007 March 6; accepted 2007 October 10)

Abstract

We present the results of multi-frequency observations of radio outbursts of the microquasar Cygnus X-3 in 2006 February and March with the Nobeyama 45-m telescope, the Nobeyama Millimeter Array, and the Yamaguchi 32-m telescope. Since the prediction of a flare by RATAN-600, the source was monitored from January 27 (UT) with these radio telescopes. At the eighteenth day after the quench of activity, successive flares exceeding 1 Jy were successfully observed. The time scale of the variability in the active phase is presumably shorter in higher frequency bands. We also present the result of a follow-up VLBI observation at 8.4 GHz with the Japanese VLBI Network 2.6 d after the first rise. A VLBI image exhibits a single core with a size of < 8 mas (80 AU). The observed image is almost stable, although the core shows a rapid variation in the flux density. No jet structure can be seen at a sensitivity of $T_{\rm b}$ (brightness temperature) $= 7.5 \times 10^5$ K.

Key words: black hole physics — radio continuum: stars — stars: variables: other

1. Introduction

Cygnus (Cyg) X-3 is a famous X-ray binary including a black-hole candidate (e.g., Schalinski et al. 1998). This object is classified as a microquasar due to its bipolar relativistic jet accompanied by radio flares. Because it is located on the Galactic plane at a distance of about 10 kpc (e.g., Predehl et al. 2000) and obscured by intervening interstellar matter, it has been observed mainly in radio and X-ray regions. Its giant radio flares have been observed once every several years since its initial discovery (Gregory et al. 1972; Braes & Miley 1972). The peak flux densities in radio flares have often increased up to levels of 10 Jy or more at centimeter wavelengths (e.g., Waltman et al. 1994). The radio emission seems to be correlated with hard X-ray emission, and not with soft X-rays (McCollough et al. 1999). Although the radio emission arises through a synchrotron process of relativistic electrons in the jet (Hjellming & Johnston 1988), a millimeter behavior during the flares has not yet been established. Observations at a shorter wavelength and with a higher time resolution are desirable to understand the mechanism of the flares.

The quenched state of Cyg X-3, in which the radio emission is suppressed below 1 mJy, is a possible precursor of flares (e.g., Waltman et al. 1994). In 2006 January, this quenched state was detected in monitoring observations with the RATAN-600 radio telescope (Trushkin et al. 2006). The source has been monitored from MJD $= 53762$ (2006 January

* The Nobeyama Radio Observatory is a branch of the National Astronomical Observatory, National Institutes of Natural Sciences, Japan.

27 in UT) with the Nobeyama 45-m radio telescope (NRO45), the Nobeyama Millimeter Array (NMA), and the Yamaguchi 32-m radio telescope (YT32). We detected the initial state, or rising phase, of the radio flare of Cyg X-3 at MJD = 53768 (2006 February 2), and observed successive flares exceeding 1 Jy (Tsuboi et al. 2006), which turned out to be the beginning of an active phase lasting more than 40 d.

In this paper, radio observations with NRO45, NMA, YT32, and the Japanese VLBI Network (JVN) are reported. The observation procedures are summarized in section 2. The light curves and the spectral evolution observed with NRO45, NMA, and YT32 are shown in section 3, together with the result of JVN. A detailed discussion based on these observations will be published as separate papers.

2. Observations and Data Reductions

2.1. Radio Photometric Observations

The first observation period was from MJD = 53763.13 (2006 January 28) to 53779.94 (2006 February 13). Observations with NRO45 of Cyg X-3 were performed alternately at 23 GHz and at both 43 and 86 GHz, simultaneously. This period corresponded to the initial phase of the radio flaring state in 2006 February–March. The second period was from MJD = 53805.12 (2006 March 11) to 53808.77 (2006 March 14). A cooled HEMT receiver with dual circular polarization feed was used at 23 GHz. SIS receivers with orthogonal linear polarization feeds were used at 43 and 86 GHz. The system noise temperatures during the observations, including atmospheric effects and antenna ohmic loss, were 80–120 K at 23 GHz, 120–200 K at 43 GHz, and 250–350 K at 86 GHz. The full width at half maximums (FWHMs) of the telescope beams are 77″ at 23 GHz, 39″ at 43 GHz, and 19″ at 86 GHz. The telescope beam was alternated between the positions of the source and sky at 15 Hz by a beam-switch in order to subtract any atmospheric effect. The antenna temperatures were calibrated by a chopper wheel method. The primary flux calibrator for conversion from antenna temperature to flux density was a proto-planetary nebula, NGC 7027, whose flux density values are given as 5.5 Jy at 23 GHz, 5.0 Jy at 43 GHz, and 4.6 Jy at 86 GHz (Ott et al. 1994). Telescope pointing was checked and corrected in every observation procedure by observing NGC 7027 in a cross-scan mode. The pointing accuracy was better than 3″ r.m.s. during these observations. The source was observed using ON-OFF observations for durations of 5–10 min, sufficient to detect and perform photometry on Cyg X-3 and the calibrator.

Interferometric observations were performed with the NMA from MJD = 53762.18 (2006 January 27) to 53776.15 (2006 February 10) at both 98 and 110 GHz simultaneously. The NMA consists of six 10 m antennas equipped with cooled DSB SIS receivers with a single linear polarization feed. The Ultra-Wide-Band Correlator with a 1 GHz bandwidth was employed for the backend (Okumura et al. 2000). The quasar 2013+370 was used as a phase and amplitude reference calibrator, and Uranus and Neptune were used as primary flux-scale calibrators. The system noise temperatures during the observations, including atmospheric effects and antenna ohmic loss, were 80–120 K at 98 GHz and 120–200 K at 110 GHz. The UV-data were calibrated with the UVPROC-II software package developed at the Nobeyama Radio Observatory (Tsutsumi et al. 1997), and then imaged with natural UV weighting, and CLEANed with the NRAO AIPS package.

Centimeter-wave observations of Cyg X-3 were also performed at 8.4 GHz for longer duration with YT32. The observation period was from MJD = 53768.29 (2006 February 2) to 53813.08 (2006 March 19). A cooled HEMT receiver was used at 8.4 GHz. The system noise temperature of YT32 during the observations, including atmospheric effects and antenna ohmic loss, was 45 K at 8.4 GHz. The primary flux calibrator for YT32 was an H II region, DR21 with a flux density of 20 Jy at 8.4 GHz. A flux measurement was carried out with an ON-OFF switching method with an overlaying small-angle offset for both the azimuth and the elevation directions. Additional observations using YT32 were also performed in 2006 May. Data at MJD = 53872 were obtained with the Mizusawa VERA Observatory 10-m radio telescope.

The uncertainty in the flux density of Cyg X-3 depends on the weather conditions. However, the sensitivity of the telescopes is not the principal factor of the uncertainty. Because the primary flux-scale calibrator for NRO45, NGC 7027, is close to Cyg X-3 in the celestial sphere, the difference in the atmospheric attenuation between these sources has no significant effect on the data. The typical systematic uncertainty is $\sim$10% for NRO45. The typical systematic uncertainty of NMA is $\sim$15%, because the primary flux-scale calibrators are not near to Cyg X-3, and the phase noise caused by atmospheric fluctuations. Although flux loss due to pointing errors is corrected by pointing offset data in the data reduction process, the uncertainty of YT32 is as much as $\sim$20%. However, the relative uncertainties of the flux density during one day should be much better than these values.

2.2. JVN Observation

A follow-up VLBI observation was carried out with the Japanese VLBI Network (JVN: K. Fujisawa et al. 2007, in preparation; Doi et al. 2006a, b). The duration of the observation was from MJD = 53770.8 to MJD = 53771.4, i.e., starting 2.6 d after the first rise of the flare. The telescopes participating in this observation were four 20-m telescopes of the VLBI Exploration of Radio Astrometry project (VERA: Kobayashi et al. 2003), Usuda 64-m (U64), Kashima 34-m (K34), YT32, and Gifu 11-m (G11). Right-circular polarization was received at 8400–8416 MHz (IF1) and 8432–8448 MHz (IF2) with a total bandwidth of 32 MHz. The VSOP/K4-terminal system was used as a digital back-end; digitized data in 2-bit quantization were recorded onto magnetic tapes at a data rate of 128 Mbps. Two sources (2000+472, 3C 454.3) other than Cyg X-3 were observed for gain and bandpass calibration, respectively. The data were correlated with the VSOP-FX correlator at the National Astronomical Observatory of Japan (Shibata et al. 1998), and fringes were detected at all baselines, except for those including the Ishigaki, Ogasawara, and G11 telescopes.

The data were reduced in the standard manner with the Astronomical Image Processing System (AIPS: Greisen 2003) developed at the US National Radio Astronomy Observatory. An amplitude-scaling factor was determined from the

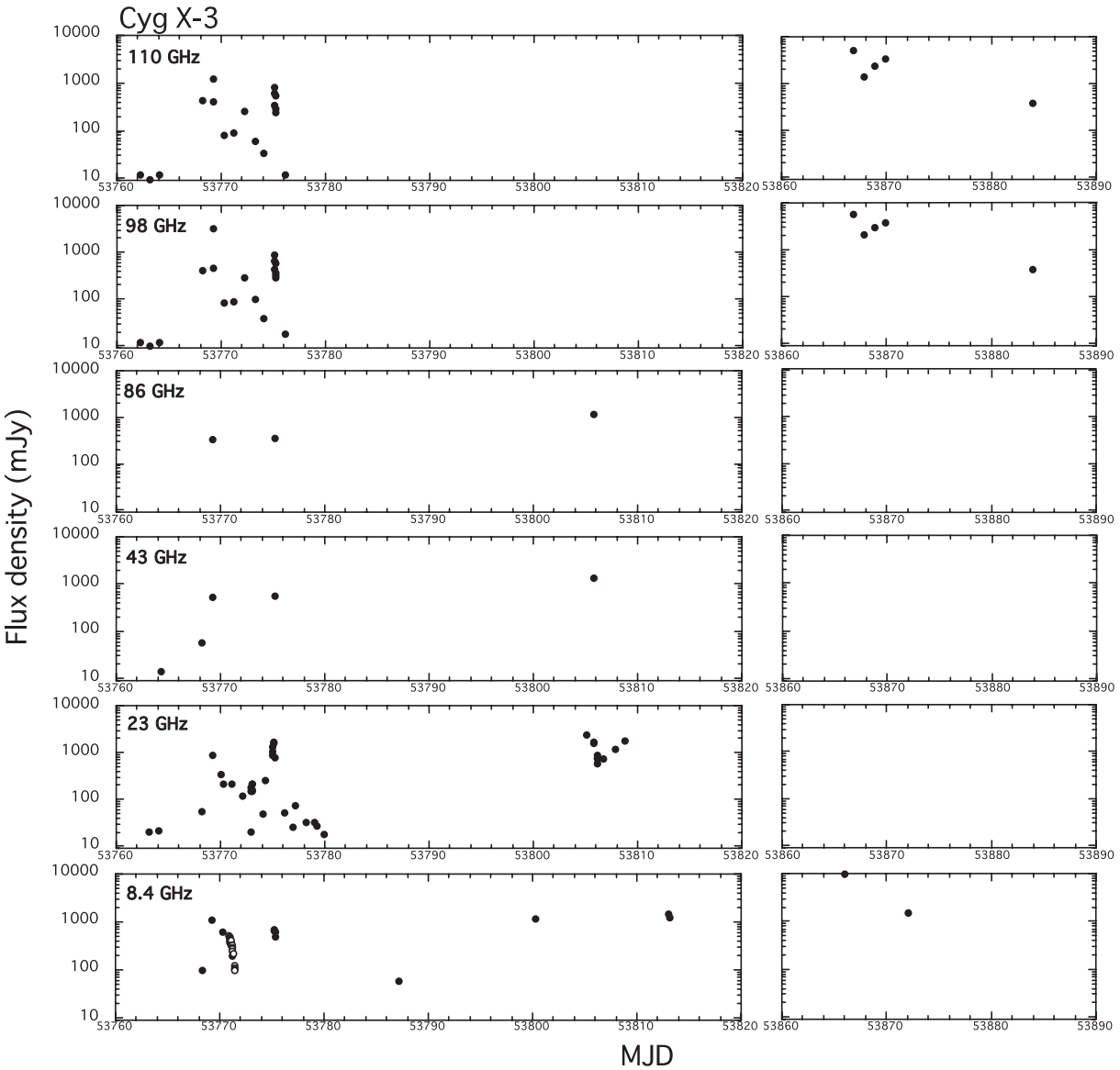

Fig. 1. Radio light curves of 2006 January to May of Cygnus X-3 at, from bottom to top, 8.4, 23, 43, 86, 98, and 110 GHz. The 8.4 GHz data were obtained with YT32. In addition, open circles at 8.4 GHz show high-density sampling flux densities observed by the Japanese VLBI Network (JVN). The 23, 43, and 86 GHz data were obtained with NRO45. The 98 and 110 GHz data were obtained with NMA. The first rise was detected at MJD = 53768.13 at 98 and 110 GHz. Within one day after the first rise, the flux density at 23 GHz also increased. The 8.4, 98, and 110 GHz data show that Cyg X-3 was in an active phase in 2006 May.

monitored system noise temperatures and the antenna efficiencies of the U64, YT32, and K34 telescopes. Furthermore, we calibrated the antenna gain variations using the data of 2000+472, which is a point source in the JVN baselines, and scanned every 30–60 min. Such a calibration method provides an absolute flux scale with an accuracy of $\sim 10\%$ and a relative time variation of the antenna gain of $\sim 3\%$ accuracy.

3. Results

3.1. Light Curves

We present the light curves of Cyg X-3 at 6 frequency bands of 8.4, 23, 43, 86, 98, and 110 GHz obtained with NRO45, NMA, and YT32 in figure 1. Table 1 summarizes the results of observations. The first rise of the flare was detected with NMA at MJD = 53768.13 or 3 am on 2006 February 2 (UT) at 98 and 110 GHz. This is about 18 d after it entered the quenched state observed with RATAN-600. The first rise was also observed at lower frequencies within 1 d. After that, we observed several peaks exceeding 1 Jy. Although there was a long intermission of observations in our campaign, the duration of the active phase of Cyg X-3 was at least over 40 d (Tosaki et al. 2006). It can be confirmed that Cyg X-3 was still active in May from the flux densities at 8.4, 98, and 110 GHz in 2006 May in figure 1 and table 1.

Figure 2a shows enlarged light curves of the initial phase of the first flare. Before the flare, the flux density of Cyg X-3 was inhibited up to a few 10 mJy at 23 to 110 GHz (see figure 1).

Table 1. Flux densities of Cyg X-3.

MJD (d)	$S_{8.4\ \mathrm{GHz}}$ (mJy)	$S_{23\ \mathrm{GHz}}$ (mJy)	$S_{43\ \mathrm{GHz}}$ (mJy)	$S_{86\ \mathrm{GHz}}$ (mJy)	$S_{98\ \mathrm{GHz}}$ (mJy)	$S_{110\ \mathrm{GHz}}$ (mJy)
53762.181					12	12
53763.125		20			10	9.6
53764.083		21			12	12
53764.208			15			
53768.125		57	58		417	442
53768.292	100					
53769.167					3247	1280
53769.208	1100	896	549	338	468	408
53770.042		339				
53770.208	650	222			85	80
53771.042		224				
53771.167	200				89	90
53772.042		122				
53772.167					288	260
53772.910		20				
53772.924		155				
53772.934		183				
53772.951		219				
53772.965		163				
53772.982		156				
53772.995		214				
53773.208					104	60
53774.042		49			39	35
53774.208		255				
53774.903		922				
53774.924		1080				
53774.937		1365				
53775.024		1732				
53775.042		1589				
53775.096					890	850
53775.104					650	620
53775.115					450	340
53775.125					300	250
53775.135					300	300
53775.140	690					
53775.146					370	300
53775.156					320	300
53775.167					590	550
53775.200	710					
53775.208		801	587	352		
53775.260	650					
53775.320	500					
53776.152		52			18	12
53776.958		25				
53777.188		74				
53778.208		33				
53778.948		34				
53779.208		29				
53779.937		18				
53787.125	60					
53800.208	1200					
53805.118		2424				
53805.729		1762				
53805.750		1609				

Table 1. (Continued)

MJD (d)	$S_{8.4\,\mathrm{GHz}}$ (mJy)	$S_{23\,\mathrm{GHz}}$ (mJy)	$S_{43\,\mathrm{GHz}}$ (mJy)	$S_{86\,\mathrm{GHz}}$ (mJy)	$S_{98\,\mathrm{GHz}}$ (mJy)	$S_{110\,\mathrm{GHz}}$ (mJy)
53805.757			1402	1203		
53806.090		805				
53806.104		896				
53806.118		733				
53806.139		601				
53806.708		764				
53807.771		1192				
53808.771		1782				
53813.000	1530					
53813.083	1260					
53866.014	10000					
53866.847					6000	5200
53867.847					2200	1400
53868.847					3000	2500
53869.847					3900	3500
53872.014	1500					
53883.847					400	400

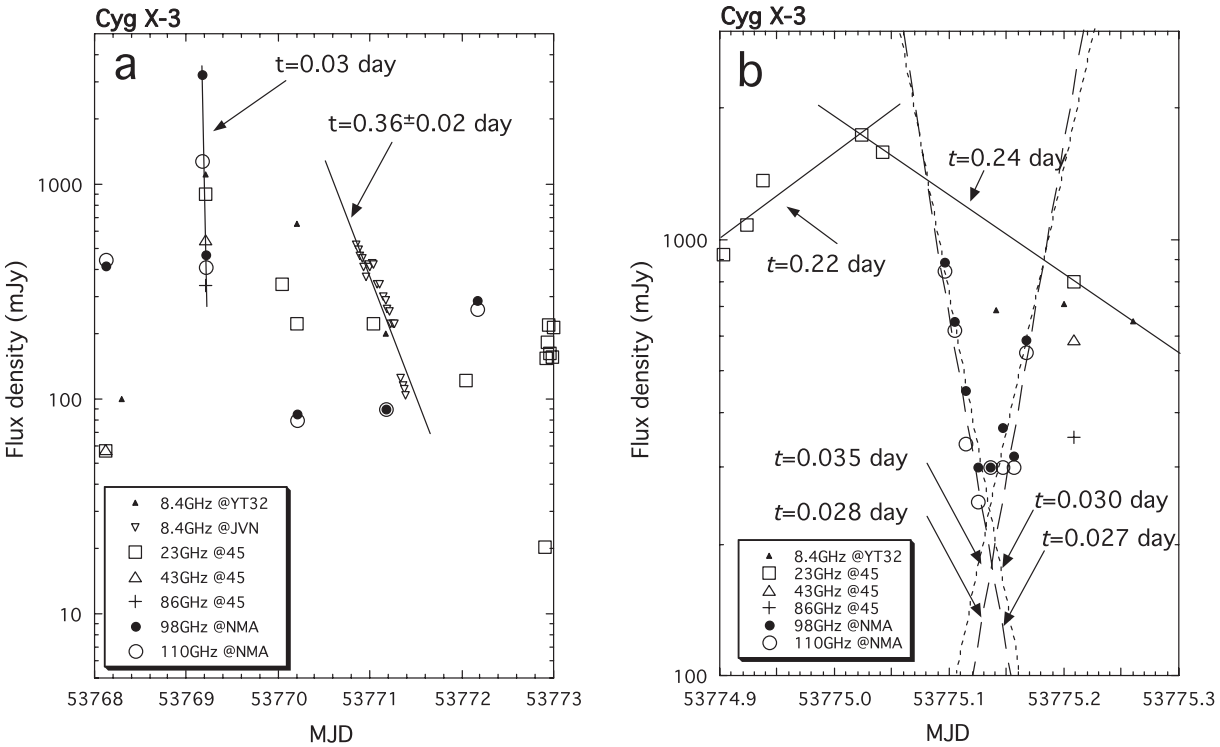

Fig. 2. Enlarged radio light curves of Cyg X-3 at the first and second flares. (a) Observation epoch is from MJD = 53768 to 53773. At MJD = 53768.13, the first rise was found by NMA at 98 and 110 GHz, and the flux densities increased up to 0.4 Jy. This is 40-times or more compared with the value before the first rise. The flux densities at MJD = 53769.17 exceeded 3 Jy at 98 GHz and 1 Jy at 110 GHz. They decreased to 1 Jy or less within one hour. The best-fitting curves of the exponential decay model are plotted in lines. The open upside-down triangles show the flux densities at 8.4 GHz observed by the Japanese VLBI Network (JVN). The flux densities at lower frequencies changed more gradually. (b) Observation epoch from MJD = 53774.9 to 53775.3. Data with NMA at 98 and 110 GHz clearly show the quench and the successive rapid rise of the millimeter flux. The best-fit curves of the exponential rise and the decay models are plotted in lines. The e-folding rise and decay times are $t \simeq 0.03$ d both at 98 and 110 GHz.

At MJD = 53768.13, the first rise was found by NMA at 98 and 110 GHz, of which the flux densities became 40-times or more compared with the value of the previous day. The flux densities at 23 and 43 GHz with NRO45 were also 3–4 times brighter than the previous values. The peak flux densities at MJD = 53769.17 exceeded 3 Jy at 98 GHz and 1 Jy at 110 GHz. They were violently variable and decreased to 1 Jy or less within one hour. Assuming an exponential decay, the

e-folding decay times would be 0.03 d both at 98 GHz and 110 GHz. On the other hand, the e-folding decay time at 8.4 GHz was $t = 0.36 \pm 0.02$ d during MJD = 53770 to 53771, which will be mentioned for details. For several major flares of Cyg X-3 observed previously, the e-folding decay times of the flux density were reported to be in the range of 0.15 to 2.75 d (Hjellming et al. 1974). The observed decay times are much shorter than these previous values.

Figure 2b shows the enlarged light curves of the second flare. We obtained a higher sampling rate light curve at 23 GHz in the rising phase of the second flare. At MJD = 53774.9, the rise of the second flare was detected at 23 GHz with NRO45. The flux density at 23 GHz increased rapidly from 0.9 to 1.7 Jy within 3 hr. This corresponds to an e-folding rise time of $t = 0.22 \pm 0.05$ d. The flux density decreased rapidly from the peak to 0.8 Jy by the next observation 4.4 hr later. If these flux densities are involved in the same flare, the e-folding decay time is $t = 0.24 \pm 0.01$ d. The decay phase of the flare was also observed at other frequencies. The flux densities observed at 98 and 110 GHz decreased rapidly within the observation interval at 23 GHz. A power law describes the decay behavior. The e-folding decay times at 98 and 110 GHz are $t = 0.030 \pm 0.003$ d and $t = 0.027 \pm 0.005$ d, respectively. These are of the same order as the first flare at 98 and 110 GHz. In addition to the peak and following decay at 23 GHz, another rising is recognized at 98 and 110 GHz in the observation break at 23 GHz. The e-folding rise times at 98 and 110 GHz are $t = 0.035 \pm 0.025$ d and $t = 0.028 \pm 0.013$ d, respectively. The e-folding rise times are also at the same level as the decay times.

Figure 3 shows the relation between the time scale of the flux variability and frequency in the 2006 flares of Cyg X-3. The e-folding rise and decay times were derived from neighboring observations within 8 hr. Our data with higher sampling rates than previous reports should reveal new information about the synchrotron jets of Cyg X-3. The e-folding time is shorter at higher frequencies, and we fit the trend with a power-law model, shown as a straight line in the figure. Although the scattering of the data points is large, the e-folding time is inversely proportional to the observed frequency, $T = 3.8 f^{-1.03}$. That cannot be explained in terms of the synchrotron bubble model, which predicts the same time scale for all the frequencies. It is suggested that the injection and loss of energy of relativistic electrons in the jet plays an important role in the spectral evolution of the flares of Cyg X-3.

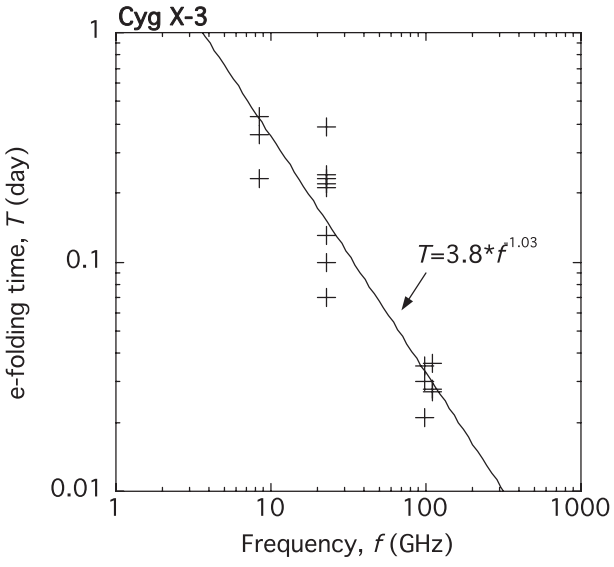

Fig. 3. Relation between the time scale of the flux variability and the frequency in the 2006 flares of Cyg X-3. The solid line is the best-fitting power-law model for these data. The e-folding time of the flux variability should inversely relate to frequency.

3.2. *Spectral Evolution of Flares*

Figure 4 shows the spectral evolution during the three days around the first flare of Cyg X-3. The curve in panel (a) indicates the spectrum at MJD = 53768.13 at the onset of the first flare. The rapid increase at 98 and 110 GHz took place first as mentioned in the previous subsection, while the flux densities at lower frequencies did not change significantly. The spectrum shows a complicated inverted feature from 43 to 98 GHz. This suggests that there is a time lag of the flare onset, depending on the frequency. The data in panel (b) indicate the flux densities at 98 and 110 GHz at MJD = 53769.17. The flux densities at 98 GHz and 110 GHz rose to 3.2 and 1.3 Jy, respectively. These are the highest values in this flare. Unfortunately, no simultaneous data at other frequencies are available. Panel (c) shows the flux densities of Cyg X-3 at MJD = 53769.21, just after 1 hr of panel (b). The flux densities at lower frequencies increased by about 10 times over the values in panel (a), but those at 98 and 110 GHz decreased dramatically in 1 hr. The spectrum is described by a power law with an index of $\alpha \simeq -0.4$. The peak flux is followed by a rapid decay at high frequency. Panel (d) shows the spectrum at MJD = 53770.21, or 1 d after the peak. The spectrum is also describable by a power law, but it was decayed to be as steep as $\alpha \simeq -0.8$. This is consistent with the decay time being shorter at higher frequency, as mentioned in the previous subsection. We assume that the spectral break seen at ~ 100 GHz at MJD = 53768.13 moves in the spectrum down to below 8 GHz in one day. This evolution of the radio spectrum may be interpreted as being the result of an adiabatic expansion of synchrotron emitting ejecta in Cyg X-3.

Figure 5 shows the spectral evolution in the three days around the second flare. Panel (a) in this figure indicates the spectrum on the day before the second peak or at MJD = 53774.04. This shows a flat spectrum with an index of -0.1, which suggests that the second flare has already started. The spectrum at another flare in March was also flat over the observation band, suggesting an optically thick radio source. A power law with an index of -0.2 can explain the spectrum. Panel (b) shows the flux densities at MJD = 53775.07. These are the highest values at 98 and 110 GHz in this flare. Following this, these decreased rapidly. However, they would be near the peak of this flare, because the value at 22 GHz reached the maximum before 1 hr. Unfortunately, it was not observed during this time at 98 and 110 GHz. Panel (c) shows the flux densities after 3 hr of panel (b); between these two panels, Cyg X-3 decreased and increased rapidly (see also figure 2b). The flux densities, except for at 8.4 GHz, were described by a power law with $\alpha \simeq -0.6$ (solid line). The spectral index was slightly steeper than that in the corresponding

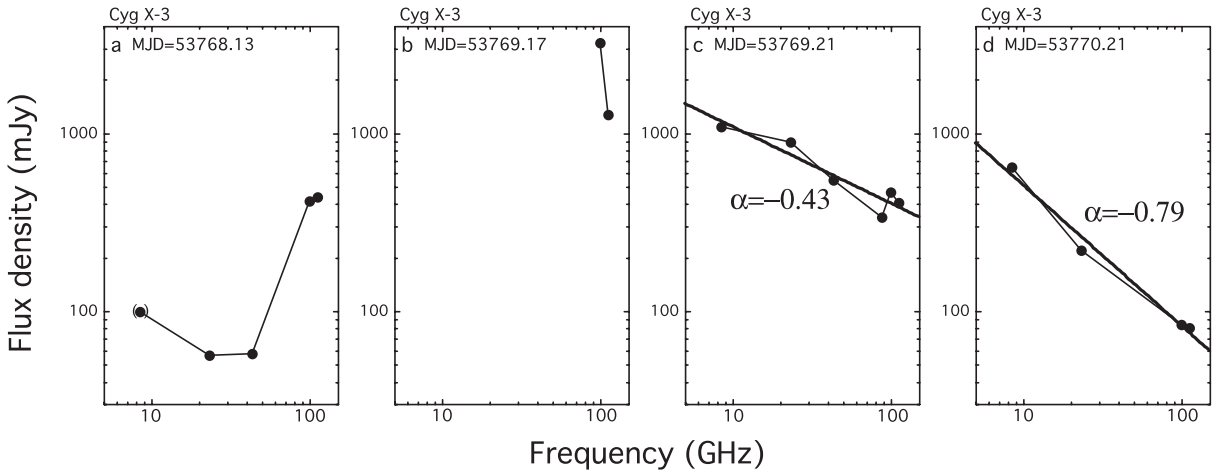

Fig. 4. Spectral evolution during the first flare. Three days evolution around the first peak at MJD = 53768. (a) On the first day at the first flare, MJD = 53768.13, the flux densities at 98 and 110 GHz increased rapidly, while the flux densities at lower frequencies were still low. (b) 98 and 110 GHz data at MJD = 53769.17. The flux densities at 98 GHz and 110 GHz were 3.2 and 1.3 Jy, respectively. These are the highest values in this flare. Unfortunately, it was not observed during this time at other frequencies. (c) Flux densities after 1 hr of panel (b). Flux densities at 8.4, 22, and 43 GHz increased by about 10 times over values in panel (a). Flux densities at 98 and 110 GHz decreased dramatically in 1 hr. A power-law model, $S \propto f^{\alpha}$, is applied to these (solid line). The best fitting of the spectral index is $\alpha \simeq -0.4$. (d) Flux densities after 1 d of panel (c). Although the flux densities were described by a power law (solid line), the spectrum was fairly steepened. The best fitting of the spectral index is $\alpha \simeq -0.8$.

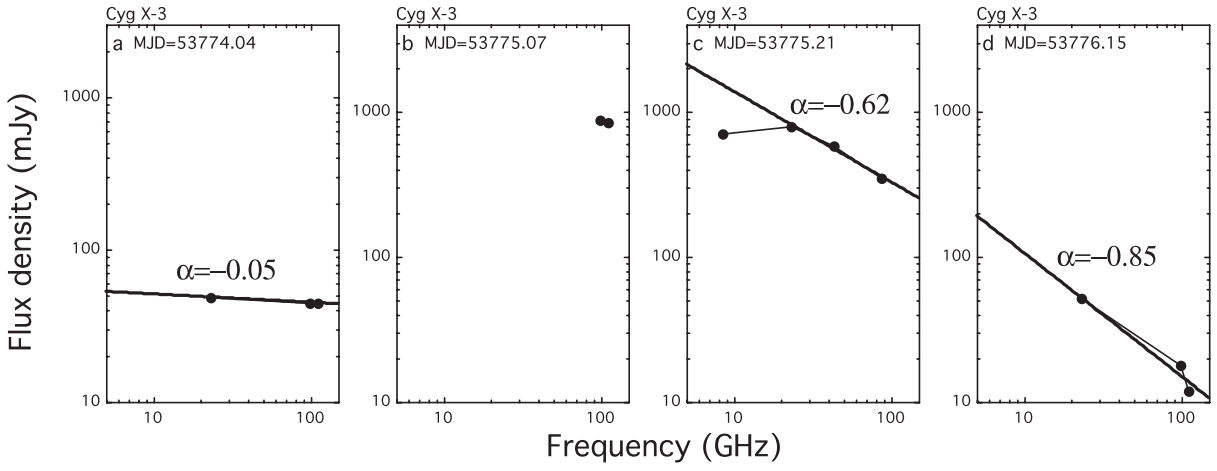

Fig. 5. Three days of spectral evolution during the second flare around MJD = 53775. (a) Flux densities one day before the second flare, or at MJD = 53774.04. The flux densities were described by a power law with $\alpha \simeq -0.1$ (solid line). (b) Flux densities at MJD = 53775.07. These are the highest values at 98 and 110 GHz in this flare. They would be near the peak of this flare, because the highest value appeared at 22 GHz before 1 hr. Unfortunately, it was not observed during this time at 98 and 110 GHz. (c) Flux densities after 3 hr of panel (b), between these two panels, Cyg X-3 decreased and increased rapidly (see also figure 2b). The flux densities, except for at 8.4 GHz, were described by a power law with $\alpha \simeq -0.6$ (solid line). (d) Flux densities after 1 d of panel (c). The spectrum was steepened. The best fitting of the spectral index is $\alpha \simeq -0.9$.

phase of the first flare. Also, panel (d) shows the flux densities after 1 d of panel (c). The spectrum was steepened. The best fitting of the spectral index is $\alpha \simeq -0.9$. The spectral index of -0.9 is similar to that one day after the first flare. The decay time of the second flare is also shorter at higher frequencies, which cannot be explained by the sole synchrotron bubble model.

3.3. 8.4 GHz VLBI Results in a Flare

Our VLBI observation started from just 2 d after the first rise of the flare, i.e., the first day after the intensity maximum of the first flare. Successive snapshots with a short integration time were made, because a rapid flux decrease was also observed during the VLBI observation. Figure 6 is an example of such a snapshot, of which the observation period was from MJD = 53770.979 to 53771.042. Only a featureless (extended) structure is found in all of the snapshot images. Deconvolution with the structure model of an elliptical Gaussian profile and self-calibration was done using DIFMAP software (Shepherd 1997). The deconvolved source size was ~ 8 mas. This is significantly broader than a synthesized beam size, 16.3 mas $\times$ 4.3 mas at PA of $-2\overset{\circ}{.}9$. However, no other component is found beyond three-times the r.m.s. of the noise of the resultant image or a brightness temperature of 7.5×10^5 K.

We also analyzed the time evolution of flux density and

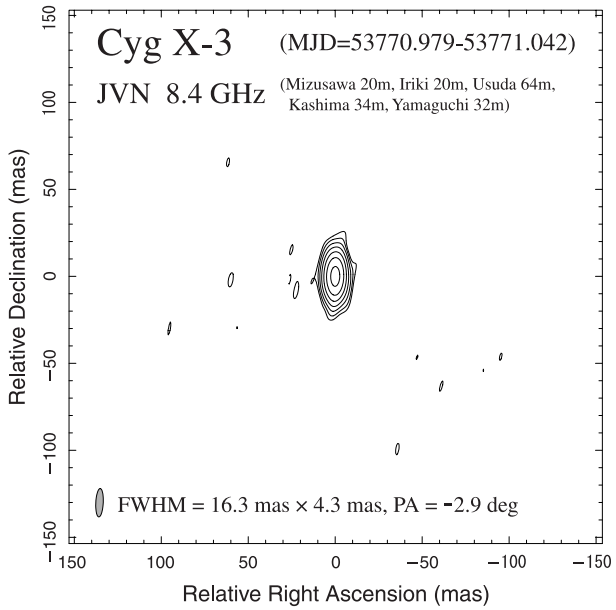

Fig. 6. Snapshot image of Cyg X-3 from VLBI data in MJD = 53770.979 to 53771.042 (1.5 hr). The beam size is 16.3 mas × 4.3 mas at PA of −2.°9, corresponding to 157 AU × 41 AU at the distance to Cyg X-3. R.m.s. of image noise, σ, is 0.70 mJy beam^{-1}. Contour levels are $3\sigma \times (-1, 1, 2, 4, 8, 16, 32, 64)$.

source structure during the JVN observation. We clipped out a series of data segments. Each segment had a duration of 1 hr, and the interval of the starting time of the segments was set to be 0.5 hr, i.e., half of a duration overlapping half of the next duration. Using the task of UVFIT in AIPS, we measured the source size and the flux density for each clipped data by visibility based model-fitting using an elliptical Gaussian profile model. The flux density of the component decreased from $\sim$500 mJy to $\sim$100 mJy during the VLBI observation lasting $\sim$14 hr (figures 2a and 7a). The source structure hardly changed, regardless of the variability of the synthesized beam (figures 7b and 7c). The weighted averages of Gaussian width (FWHM) along the major axis, along the minor axis, and the position angles of the major axis of the source structure are 8.9 ± 0.1 mas, 7.1 ± 0.1 mas, and $15.^{\circ}0 \pm 2.^{\circ}3$, respectively, i.e., we have resolved the source, which is slightly but significantly elongated in a north–south direction. Our VLBI observation has revealed that Cyg X-3 showed no significant structure change, in spite of the rapid flux variability at 8.4 GHz during the period.

Previous studies (Miller-Jones et al. 2004) showed that the two-sided jets were ejected toward north and south after major radio flares. If the ejection was concurrent with the first rise of the flux, and the jet axis was fairly close to perpendicular to the line of sight, the traveling distance of the ejecta is expected to be 350 AU or 35 mas at 10 kpc. However, we have not found any evidence of such a jet structure. The source size in our VLBI image is presumably affected by interstellar scattering, because it is consistent with the expected scattering size at 8.4 GHz (Schalinski et al. 1995). Thus, there is no structural evolution on a scale of larger than 5 mas in spite of rapid flux variability. That may be a strong constraint on jet evolution during a few days after a radio flare.

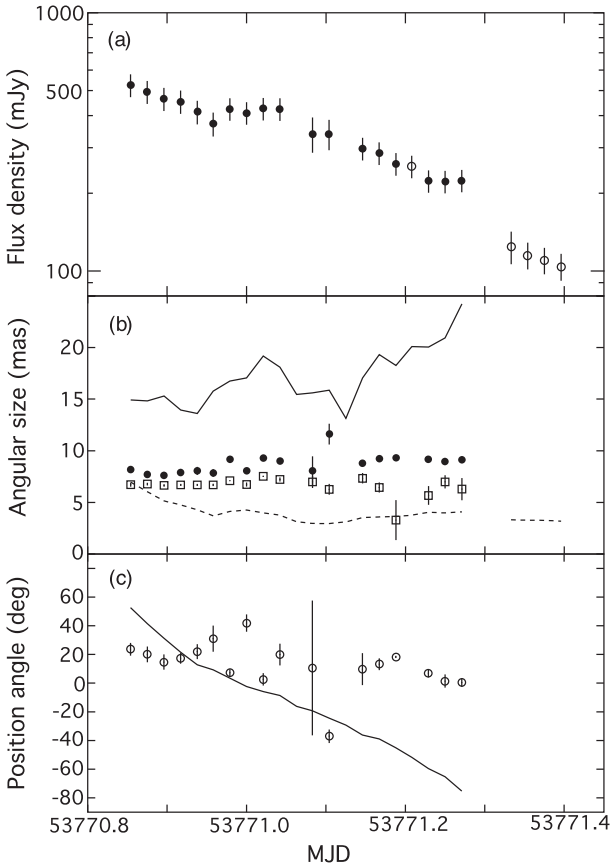

Fig. 7. Evolution of the source structure of Cyg X-3 obtained with VLBI. A series of measurements was performed by a visibility based model-fitting using an elliptical-Gaussian profile model with free parameters of the flux density, the FWHMs along the major and minor axes, and the position angle of the major axis (see text in detail). (a) Flux densities of the VLBI component (filled circles). The open circles represent measurements using a circular-Gaussian model, rather than an elliptical one, due to poor data quality. (b) Angular sizes of fitted source structure. The filled circles and open squares represent the FWHMs along the major and minor axes, respectively. The solid and dashed lines represent the major and minor axes of HPBWs of a synthesized beam in uniform-weighting, for a comparison. (c) Position angles of the major axis of the fitted source structure (open circles). The solid line represents the position angle of the major axis of synthesized beam, for a comparison.

The authors would like to thank the members of the NRO45 group and the NMA group of Nobeyama Radio Observatory for support in the observations. This work is partially supported by the Japan–Russia Research Cooperative Program of Japan Society for the Promotion of Science. The studies are partially supported by the Russian Foundation Base Research (RFBR) grant N 05-02-17556 and the mutual RFBR and Japan Society for the Promotion of Science (JSPS) grant N 05-02-19710. The JVN project is led by the National Astronomical Observatory of Japan (NAOJ), which is a branch of the National Institutes of Natural Sciences (NINS), Hokkaido University, Gifu University, Yamaguchi University, and Kagoshima University, in cooperation with the Geographical Survey Institute (GSI), the Japan Aerospace Exploration Agency (JAXA), and the National Institute of Information and Communications Technology (NICT). TK is supported

by a 21st Century COE Program at Tokyo Tech "Nanometer-Scale Quantum Physics" by the Ministry of Education, Culture, Sports, Science and Technology.

References

Braes, L. L. E., & Miley, G. K. 1972, Nature, 237, 506
Doi, A., et al. 2006a, in Proc. of the 8th European VLBI Network Symposium, ed. B. Willem et al. (Trieste: Proceedings of Science), 71 (astro-ph/0612528)
Doi, A., et al. 2006b, PASJ, 58, 777
Gregory, P. C., Kronberg, P. P., Seaquist, E. R., Hughes, V. A., Woodsworth, A., Viner, M. R., & Retallack, D. 1972, Nature, 239, 440
Greisen, E. W. 2003, in Information Handling in Astronomy — Historical Vistas, ed. A. Heck (Dordrecht: Kluwer), 109
Hjellming, R. M., Brown, R. L., & Blankenship, L. C. 1974, ApJ, 194, L13
Hjellming, R. M., & Johnston, K. J. 1988, ApJ, 328, 600
Kobayashi, H., et al. 2003, ASP Conf. Ser., 306, 367
McCollough, M. L., et al. 1999, ApJ, 517, 951
Miller-Jones, J. C. A., Blundell, K. M., Rupen, M. P., Mioduszewski, A. J., Duffy, P., & Beasley, A. J. 2004, ApJ, 600, 368
Okumura, S. K., et al. 2000, PASJ, 52, 393
Ott, M., Witzel, A., Quirrenbach, A., Krichbaum, T. P., Standke, K. J., Schalinski, C. J., & Hummel, C. A. 1994, A&A, 284, 331
Predehl, P., Burwitz, V., Paerels, F., & Trümper, J. 2000, A&A, 357, L25
Schalinski, C. J., et al. 1995, ApJ, 447, 752
Schalinski, C. J., et al. 1998, A&A, 329, 504
Shepherd, M. C. 1997, in ASP Conf. Ser. 125, Astronomical Data Analysis Software and Systems VI, ed. G. Hunt & H. E. Payne (San Francisco: ASP), 77
Shibata, K. M., Kameno, S., Inoue, M., & Kobayashi, H. 1998, ASP Conf. Ser. 144, in IAU Colloq. 164, Radio Emission from Galactic and Extragalactic Compact Sources, ed. J. A. Zensus, G. B. Taylor, & J. M. Wrobel (San Francisco: ASP), 413
Tosaki, T., Nakanishi, K., Tsuboi, M., Trushkin, S., Kameya, O., Fujisawa, K., Kotani, T., & Kawai, N. 2006, ATel, 952, 1
Trushkin, S. A., Nizhelskij, N. A., Bursov, N. N., & Majorova, E. K. 2006, in IAU Symp. 238, 463
Tsuboi, M., et al. 2006, ATel, 727, 1
Tsutsumi, T., Morita, K.-I., & Umeyama, S. 1997, in ASP Conf. Ser. 125, Astronomical Data Analysis Software and Systems VI, ed. G. Hunt & H. E. Payne (San Francisco: ASP), 50
Waltman, E. B., Fiedler, R. L., Johnston, K. J., & Ghigo, F. D. 1994, AJ, 108, 179